Advances in Science and Technology Research Journal

Advances in Science and Technology Research Journal, 2026, 20(10), 282–296
https://doi.org/10.12913/22998624/224844
ISSN 2299-8624, License CC-BY 4.0

Received: 2026.05.21
Accepted: 2026.07.19
Published: 2026.09.01

Assessment of GPS/EGNOS positioning integrity and accuracy at a small airfield using a local protection level model

Karolina Sobecka[1*], Grzegorz Grunwald[1], Adam Ciećko[1], Kamil Krasuski[2]

[1] Faculty of Geoengineering, University of Warmia and Mazury in Olsztyn, ul. Oczapowskiego 2, 10-720 Olsztyn, Poland
[2] Faculty of Navigation and Logistic, Polish Air Force University, ul. Dywizjonu 303 nr 35, 08-521 Dęblin, Poland
* Corresponding author's e-mail: karolina.sobecka@doktorant.uwm.edu.pl

ABSTRACT

The article analysed the possibility of using the European Geostationary Navigation Overlay Service (EGNOS) system as an extension of GNSS systems in landing procedures at small airports and landing sites without classic ground infrastructure. The aim of the study was to assess the positioning accuracy and integrity protection levels (HPL and VPL) in selected Global Navigation Satellite System (GNSS) signal reception configurations, including autonomous GPS, multi-system systems (GPS/GLONASS, GPS/Galileo/BeiDou, Full GNSS) and Satellite-Based Augmentation System (SBAS) modes: EGNOS non-precision approach (NPA) and EGNOS precision approach (PA). The measurements were carried out using a Septentrio PolaRx5e GNSS surveying receiver located at the Gryźliny landing site (EPGR). The observational data were processed using the Septentrio PP-SDK software and then subjected to statistical and graphical analysis, taking into account positioning parameters, such as position error distribution over time, horizontal and vertical accuracy (HPE, VPE), geometric coefficients (PDOP), and confidence levels (HPL, VPL). In addition, the article includes an analysis of cumulative distribution functions (CDF), Stanford plots, relative rHPL and rVPL indicators, and the Local Protection Level Model (LPLM) developed as part of this work. The results obtained clearly show that the configurations supported by the EGNOS system significantly improve positioning accuracy and provide greater stability compared to autonomous modes. The EGNOS system is therefore a reliable and effective tool for implementing the GNSS-based approach procedures at small airports, in accordance with the ICAO standards for performance-based navigation.

Keywords: GNSS, EGNOS, HPL, VPL, integrity, protection levels, LPLM, general aviation.

INTRODUCTION

Over the past few years, the evolution of GNSS technology has led to its widespread use in civil aviation, providing support for flight operations around the world [1,2]. The solutions based on global navigation satellite systems enable navigation in all phases of flight, often without the need for traditional ground infrastructure [3,4]. The ever-increasing accuracy, global coverage, and wide availability of these systems mean that the GNSS technologies are also increasingly being used at small airports and landing sites [5,6]. This approach contributes to increased airspace availability, improved operational safety, and more efficient air traffic management, especially under complex and demanding operating conditions [7].

Despite the high level of technical advancement and numerous advantages of GNSS, autonomous satellite systems are not able to independently meet the stringent requirements set by the International Civil Aviation Organization (ICAO) in terms of accuracy, integrity, availability, and signal continuity [8,9], especially with regard to vertical approach procedures (APV) [10]. To meet these requirements, Satellite-Based

Augmentation Systems (SBAS) have been developed to provide real-time correction data and information on GNSS signal reliability [11,12], enabling its safe use in aviation operations.

In European airspace, the EGNOS (European Geostationary Overlay Service) [13,14] acts as an augmentation system. The system was designed to increase the accuracy and integrity of positioning [15]. The integration of EGNOS with the GPS system allows civil users to perform approach procedures, such as NPA (Non-Precision Approach), APV-I (Approach Procedure with Vertical Guidance) or LPV 200 (Localiser Performance with Vertical Guidance) without the need for ground infrastructure such as ILS [10,16]. Despite its availability and certification for aviation applications, the potential of EGNOS remains untapped, especially at small airports and airfields, where its implementation could bring the greatest practical benefits, increasing the safety and availability of aviation operations without incurring high costs [17].

The current state of research in the field of EGNOS mainly includes analyses of the system's quality parameters conducted at large airports and during test flights [14,18]. The results of the work carried out so far confirm the effectiveness of the SBAS systems under such conditions, indicating an improvement in GNSS signal integrity, stability of protection levels, and ensuring the operability of LPV procedures [19,20]. Research on the functioning of EGNOS at small, uncontrolled landing sites without classic ground infrastructure is much less common. The available literature also lacks studies devoted to the analysis of local protection levels and their dependence on actual position errors in static measurements [21,22]. In response to this research gap, the study proposed an original local protection level model (LPLM), which enables the analytical determination of protection levels based on standardised position errors and geometric parameters [23,24]. The model allows assessing whether the solutions without SBAS support can meet the ICAO requirements and to what extent the EGNOS system can realistically support the implementation of approach procedures at small airports.

The aim of this article was to evaluate the effectiveness of the EGNOS system using the example of the small, uncontrolled Gryźliny (EPGR) landing site located in Poland. The research was conducted based on measurement data recorded using a Septentrio PolaRx5e GNSS surveying receiver [25]. The analysis takes into account various satellite signal reception configurations, including autonomous GPS mode, multi-system configurations (GPS/GLONASS, GPS/Galileo/BeiDou and Full GNSS), and EGNOS operating modes corresponding to NPA and PA procedures [16,26]. The positioning accuracy parameters (HPE, VPE), geometric coefficients (PDOP), and integrity protection levels (HPL, VPL) were evaluated, and an integrity analysis was performed based on Stanford plots and the cumulative distribution function (CDF). The whole is complemented by an analysis of relative indicators rHPL and rVPL and the author's proposal – LPLM.

RESEARCH METHODS AND TOOLS

The research was conducted at the uncontrolled Gryźliny landing site (EPGR) (Figure 1), located in the Warmian-Masurian Province, south of Olsztyn (Poland). The facility is a typical example of local aviation infrastructure without a certified ground radio station. Such landing sites mainly serve general aviation, which increasingly relies on GNSS systems as one of the primary sources of aircraft position information [1,3]. It is worth noting that the modern landing field was created on the site of the former German military airport Fligerhorst Grieslinen, which was operational at the beginning of World War II. After the end of World War II, the facility was decommissioned and reactivated as a civil landing field in 2007. Due to limited technical resources and the lack of ground infrastructure, this facility provides a suitable environment for analysing the application of SBAS systems [11,13].

The measurement data was obtained during a 24-hour measurement session conducted on May 8, 2024, using a Septentrio PolaRx5e geodetic receiver (Figure 2) [25]. The device enables simultaneous reception of GNSS signals from multiple constellations and at different frequencies. The measurement was performed in static mode, with a data recording frequency of 1 Hz, using a multi-frequency GNSS antenna. The 24-hour data recording time enabled the analysis of satellite geometry variability and the quality of GNSS signal parameters under real conditions [21,22].

The collected observation data was pre-processed using the PP-SDK processing module developed by Septentrio [27]. Raw measurements saved in SBF (Septentrio Binary Format) were converted to the standard RINEX format, saved as

Figure 1. GNSS monitoring station located at the Gryźliny landing site (EPGR)

Figure 2. Septentrio PolaRx5e receiver installed at the Gryźliny landing site (EPGR)

ASCII files. The conversion enabled further analysis. At this stage, the coordinates of the positions in the geocentric system (XYZ) and a set of positioning quality parameters were extracted [28,29]. The analysed values included, among others, horizontal and vertical accuracy (HPE, VPE), cumulative distribution functions (CDF), geometric coefficients (PDOP), number of visible satellites, as well as integrity protection levels (HPL, VPL) in the case of the configurations with an active SBAS system [23,24]. In addition, some of the statistical calculations and all of the graphical processing were performed in the Python environment.

The study considered six different GNSS signal reception configurations:

- autonomous GPS,
- GPS + GLONASS,
- GPS + Galileo + BeiDou,
- Full GNSS (all systems combined),
- EGNOS in non-precision approach (NPA) mode,
- EGNOS in precision approach (PA) mode.

For each configuration considered, a comparative analysis of the above-mentioned positioning quality parameters was performed. An important aspect was the assessment of the compliance of the specified integrity protection levels with the requirements specified by ICAO for the NPA and APV-I approach procedures [8,10]. In order to deepen the analysis of positioning errors, the receiver coordinates were compared with the reference coordinates, and the differences obtained were converted to the local topocentric ENU (East-North-Up) system [28,30]. On this basis, the horizontal position error (HPE) and vertical position error (VPE) were determined.

The study also proposed an original LPLM for assessing the integrity of GNSS configurations without SBAS support. The model allows local protection levels to be determined based on an analysis of position errors and geometric coefficients [23,24]. The values obtained in the model allow the operational capability of the system to be verified in relation to the ICAO standards [9,10].

RESULTS AND DISCUSSION

Analysis of positional error accuracy (HPE, VPE) over time

The precisely known position of the reference station located at the Gryźliny landing field (EPGR) served as a reference point, relative to which position differences were determined for each measurement epoch. The determined differences were transformed into the local ENU (East-North-Up) system [28,30].

On this basis, the following were determined:

Horizontal position error (HPE) – as the difference in distance between the determined position and the reference position.

$$HPE = \sqrt{E^2 + N^2} \quad (1)$$

where: E – error in the eastern direction, N – error in the northern direction.

Vertical position error (VPE) – as the absolute value of the difference between the determined height and the reference height.

$$VPE = |U| \quad (2)$$

where: U – error in the vertical direction.

The following formulas were used to calculate the basic statistics of position errors, determining their stability and variability over time [35].

Average error value:

$$\overline{HPE} = \frac{1}{n}\sum_{i-1}^{n} H_i,\ \overline{VPE} = \frac{1}{n}\sum_{i-1}^{n} V_i \quad (3)$$

Root mean square (RMS) value:

$$RMS_{HPE} = \sqrt{\frac{1}{n}\sum_{i-1}^{n}(H_i)^2},$$

$$RMS_{VPE} = \sqrt{\frac{1}{n}\sum_{i-1}^{n}(V_i)^2} \quad (4)$$

where: $\overline{HPE}$, $\overline{VPE}$ – average error value, H_i, V_i – value at a given measurement time instant i, n – number of epochs.

The RMS indicator is one of the most reliable statistics for assessing positioning quality due to its ability to provide a general description of the error level in the entire measurement set, while taking into account the influence of extreme values [31,32].

Based on the presented calculation formulas, the characteristics of HPE and VPE errors were determined for all analysed variants. The obtained values are summarised in Table 1, while the course of errors over time is presented in the summary chart. The graphical presentation of the results allows for a direct comparison of position stability between individual configurations.

The statistical analysis presented in Table 1 is supplemented by a graphical representation of the variability of horizontal errors (Figure 3) and vertical errors (Figure 4) over time.

Table 1. Summary of position error statistics (HPE, VPE) for the analysed GNSS configurations

Variant type	Maximum error [m]		Mean error [m]		RMS error [m]	
	Horizontal	Vertical	Horizontal	Vertical	Horizontal	Vertical
EGNOS NPA	1.008	1.738	0.456	0.346	0.489	0.459
EGNOS PA	1.010	1.734	0.456	0.345	0.489	0.458
GPS	1.452	2.801	0.725	0.895	0.785	1.121
GPS/GLONASS	1.364	3.018	0.709	0.906	0.762	1.146
GPS/Galileo/BeiDou	4.198	25.094	0.801	3.856	0.950	5.956
FULL GNSS	2.359	15.083	0.694	2.844	0.779	4.271

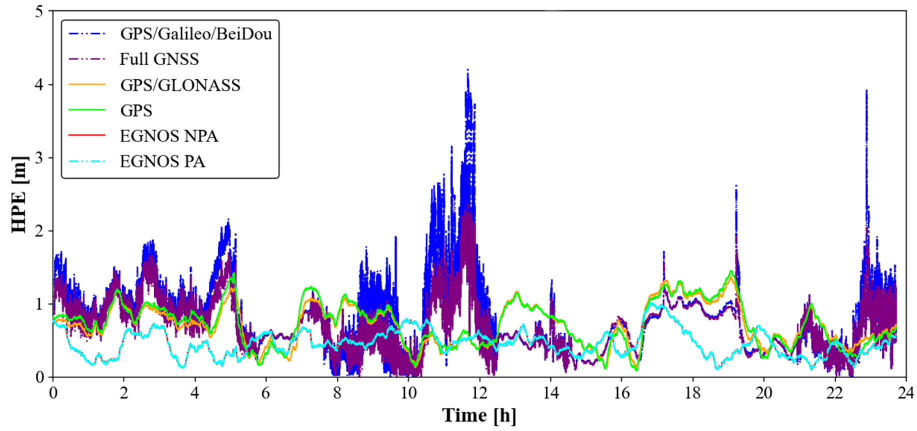

Figure 3. Variability of horizontal position errors (HPE) over time for the analysed GNSS configurations

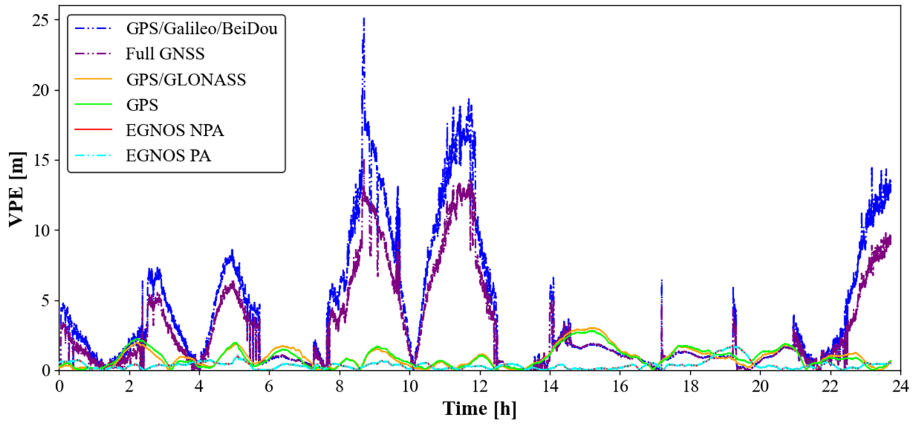

Figure 4. Variability of vertical errors (VPE) over time for the analysed GNSS configurations

The results obtained showed a clear advantage of the EGNOS-supported configurations over autonomous and multi-system solutions. In the EGNOS NPA and EGNOS PA modes, horizontal error values remained at 0.3–0.6 m for most of the time, while vertical errors did not exceed 1.0–1.5 m during the entire measurement session. In autonomous and multi-GNSS solutions, greater error variability and periodic increases in error values were observed, especially in the vertical direction. For the GPS/Galileo/BeiDou and Full GNSS variants, numerous increases in VPE were recorded, reaching 10–15 m, and locally even above 20 m. In the horizontal plane, errors in these variants mostly reached 1.5–2.0 m with periodic increases to 3–4 m. The observed differences confirm that the lack of an augmentation system leads to a reduction in the stability and quality of the determined position. The use of the EGNOS system results in a significant reduction in error variability and an improvement in positioning accuracy and stability.

Statistical analysis of position errors – CDF

Analysis of positioning errors based on time history allows the dynamics of HPE and VPE errors to be determined. However, from the point of view of aviation applications, analysis of the full statistical distribution of errors is also important [32,33]. For the purposes of landing approach procedures, information on how often the positioning error value remains below certain thresholds is essential, as it directly affects the assessment of the stability and integrity of the GNSS/EGNOS system [9,10]. For this purpose, cumulative distribution functions (CDF) were used to describe the probability of meeting the following condition. CDF, being a cumulative form of a histogram, provides insight into the statistical distribution of positioning errors:

$$P(HPE \leq h), P(VPE \leq v) \qquad (5)$$

for the accepted error thresholds h and v. The CDF function takes values from 0 to 1 (0–100%)

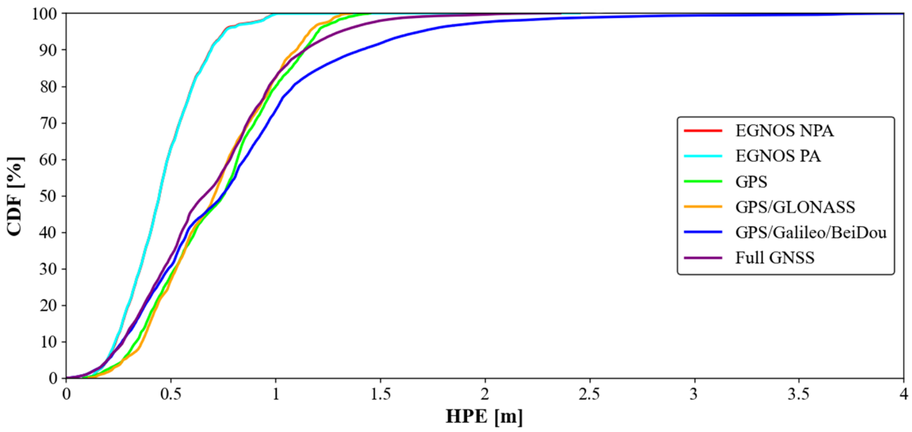

Figure 5. Cumulative distribution function (CDF) of horizontal error (HPE) for the analysed GNSS configurations

and allows comparison of the proportion of measurement epochs in which individual configurations achieve a specified positioning quality [31].

The cumulative CDF function is defined as:

$$CDF_{HPE}(h) = \frac{1}{n}\sum_{i=1}^{n} I(HPE_i \leq h),$$

$$DF_{VPE}(v) = \frac{1}{n}\sum_{i=1}^{n} I(VPE_i \leq v) \quad (6)$$

where: HPE_i and VPE_i denote the positioning error values in the i-th measurement epoch, n is the number of epochs, and $I(HPE_i \leq h)$ or $I(VPE_i \leq h)$ is an indicator function that takes the value 1 if the condition is met or 0 if the condition is not met.

The adopted definition of the CDF function allows comparing the behaviour of individual GNSS configurations across the full range of error values observed. The rest of the analysis presents separate graphs illustrating the cumulative functions of horizontal (Figure 5) and vertical (Figure 6) errors [32,33].

The graph shows that EGNOS-supported systems are characterised by the highest proportion of small horizontal errors. For the EGNOS PA and EGNOS NPA modes, over 90% of observations are below 1.0 m. For the other systems, wider CDF curves can be observed, indicating greater error variability.

In the case of vertical errors, the variation in errors is more pronounced. The EGNOS-supported systems achieve over 95% of observations with an error below 1.0 m. In contrast, for the other configurations, a distribution with significantly greater dispersion and increased error variability is visible. Analysis of the cumulative function graphs clearly confirms that the EGNOS system improves the stability of positioning errors in both planes. The configurations with an active augmentation system show a high probability of minor errors. Autonomous and multi-GNSS solutions show a clearly wider error distribution and the presence of increased extreme values.

PDOP coefficient analysis

Satellite geometry is one of the basic factors determining the quality of GNSS solutions [34,35]. The analysis assessed the daily variability of the PDOP coefficient, commonly used as a measure of satellite geometry quality [36]. Lower PDOP values reflect a more favourable satellite configuration and contribute to a more stable positioning solution.

The receiver determines PDOP values in accordance with the internal implementation of geometric algorithms, while the definition commonly used in the literature is presented below.

PDOP values are determined based on the satellite geometry matrix G and can be described by the following equation:

$$PDOP = \sqrt{\sigma_x^2 + \sigma_y^2 + \sigma_z^2} \quad (7)$$

where: the components $\sigma_x^2 + \sigma_y^2 + \sigma_z^2$ denote the diagonal elements of the covariance matrix: $(G^T G)^{-1}$ [34,35].

For each variant, the daily variability of the PDOP coefficient was analysed in relation to the number of available satellites [29,35]. The

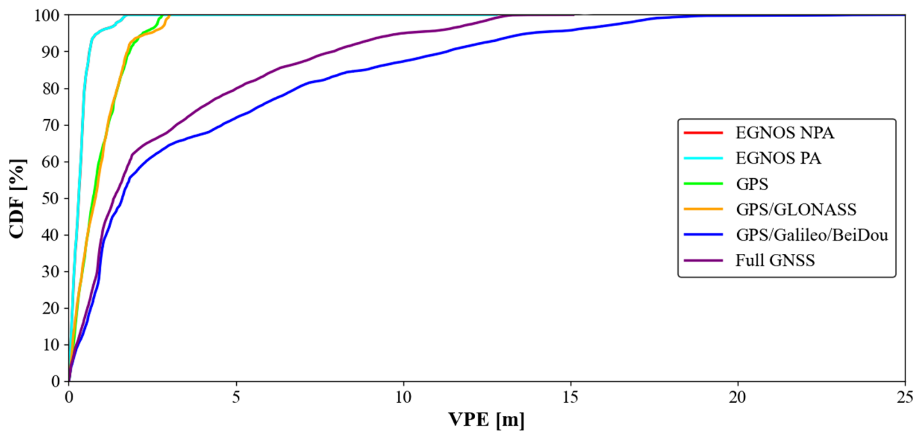

Figure 6. Cumulative distribution function (CDF) of vertical position error (VPE) for the analysed GNSS configurations

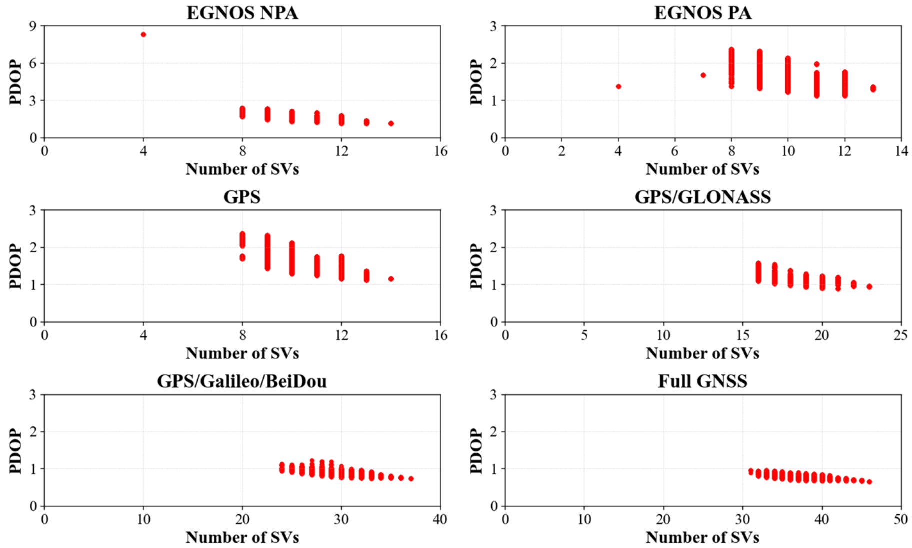

Figure 7. Relationship between PDOP and number of satellites

analysis made it possible to assess the impact of the EGNOS augmentation system on the geometry and stability of position determination [38]. The results are presented in comparative graphs (Figure 7), showing the relationship between the PDOP value and the number of available satellites.

Analysis of PDOP indicates differences in geometric conditions between the GNSS configurations considered. The most favourable geometric conditions were observed for the Full GNSS variant, resulting from the large number of available satellites and their even distribution. The solutions based solely on GNSS are characterised by greater variability in PDOP values, while in the case of the modes with an active EGNOS system, the values of the coefficient remained relatively low, despite the limited number of visible satellites.

Analysis of protection levels (HPL, VPL)

The horizontal protection level (HPL) and vertical protection level (VPL) are among the basic parameters used in the integrity analysis of GNSS and SBAS systems [23,37]. They define the maximum acceptable position error that should not be exceeded at a given confidence level (e.g., 99.999%). In aviation applications, protection levels are particularly important because the HPL and VPL values determine the eligibility of a navigation system for the NPA and APV approach procedures, in accordance with the applicable ICAO requirements [8,10].

In general terms, protection levels can be expressed as [37,38]:

$$HPL = k_H \cdot \sigma_H, VPL = k_V \cdot \sigma_V \tag{8}$$

where: σ_H, σ_V – standard deviation of vertical and horizontal positions, determined on the basis of the covariance matrix of the solution, k_H, k_V – integrity coefficients depending on the required level of integrity.

In the case of PA (APV) approach procedures, the typical values of the coefficients $k_H = 6.0$ and $k_V = 5.33$ are assumed, resulting from the assumed integrity risk of 10^{-7} per approach [10,37]. For the NPA procedure, only the horizontal plane is analysed, for which the coefficient $k_H = 6.18$ is used [8]. In the solutions supported by the EGNOS system, the HPL and VPL protection levels are determined based on advanced integrity assessment algorithms [11,13]. The algorithms use orbit and satellite clock corrections, ionospheric delay models, and uncertainty indicators [14,39]. The standard deviations σ_H and σ_V result from a weighted covariance matrix. The protection levels determined by the EGNOS system are certified and can be used operationally in civil aviation [10].

In the case of autonomous GNSS solutions, protection levels are not provided by an external augmentation system. The GNSS receiver estimates them independently using RAIM (Receiver Autonomous Integrity Monitoring) algorithms [24,37]. The covariance matrix results from the geometry of the satellites, and the *k* coefficient depends on the adopted static test parameters [40]. The obtained protection levels are purely computational, are not certified, and cannot be used operationally. In autonomous solutions, the relationship between position accuracy and satellite geometry can be approximated using the HDOP and VDOP coefficients [34,36]:

$$HPL \approx k_H \cdot HDOP \cdot \sigma_\rho, VPL \approx k_V \cdot VDOP \cdot \sigma_\rho \quad (9)$$

where: *HDOP*, *VDOP* – geometric coefficients determining the impact of satellite geometry on the accuracy of the determined position, σ_ρ – standard deviation of pseudorange error.

The above relationship is simplified and is mainly used in autonomous GNSS solutions. In SBAS systems, protection levels are based on extended error models and are not directly related to the DOP·σρ relationship [11,39].

For the purposes of analysis, the protection levels determined for the solutions without EGNOS support are treated solely as qualitative indicators for assessing the relationship between the actual position error and the available safety margin [23,38]. In turn, the values obtained in the NPA and PA modes allow the EGNOS system's performance in local conditions to be assessed [13,14]. A summary comparison of HPL and VPL variability over time for the analysed measurement variants is shown in Figure 8.

Analysis of daily protection level variability showed a clear advantage of the solutions using the EGNOS system over autonomous and multi-GNSS solutions. In the EGNOS NPA and EGNOS PA modes, the HPL values remained stable at around 6–10 m, while the VPL values did not exceed 15–20 m during the entire measurement session. The EGNOS PA mode performed best, with the lowest HPL and VPL variability and high resistance to short-term disturbances. For the other systems, the protection levels were significantly higher: HPL at around 10–12 m, while VPL increased to 15–22 m. The results clearly confirm that the solutions supported by the EGNOS system provide stable protection levels. The other variants show greater variability and susceptibility to error growth, limiting their usefulness in operations requiring a high level of integrity.

Relative indicators (rH_{PL}, rV_{PL})

A correct assessment of the integrity of GNSS systems requires consideration of the interdependencies between actual position errors and protection levels [23,38]. For this purpose, two relative indicators, rH_{PL} (horizontal) and rV_{PL} (vertical), were used, the main task of which is to determine the degree of utilisation of protection levels by the actual position error. Relative indicators are commonly used in GNSS integrity studies, while in the present analysis they were used to assess the stability and integrity of the signal reception variants under consideration. Relative protection level indicators are defined as the ratio of position errors to the corresponding integrity protection level [8]:

$$rH_{PL} = \frac{HPE}{HPL}, rV_{PL} = \frac{VPE}{VPL} \quad (10)$$

where: *HPE*, *VPE* – actual horizontal and vertical position errors, *HPL*, *VPL* – integrity protection levels determined by the GNSS receiver.

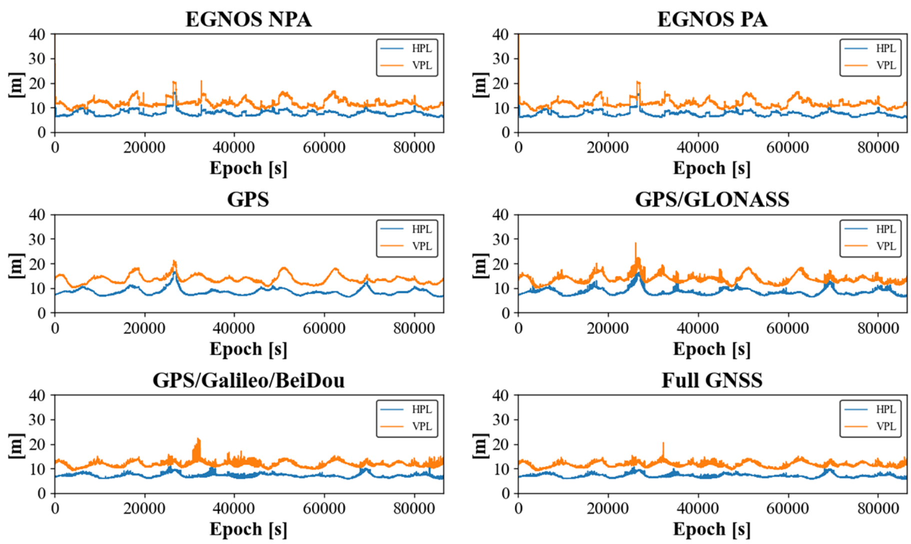

Figure 8. HPL and VPL variability over time for each measurement variant

The interpretation of the relative rH_{PL} and rV_{PL} values is as follows:
- Values below 1 indicate that the actual position errors are within the specified protection levels. This means that the system integrity is maintained in accordance with the ICAO requirements for air operations [8].
- Values close to 1 mean that the position error reaches the acceptable limit, and the available safety margin is minimal. The system operates under conditions of increased sensitivity to interference.
- Values exceeding 1 indicate that the specified protection level has been violated, which indicates a potential loss of system integrity [37].

The relative indicators used made it possible to compare the behaviour of individual GNSS configurations in terms of position error stability and the degree of safety margin utilisation in the horizontal and vertical component [23]. Statistical analysis of rH_{PL} and rV_{PL} waveforms allowed for a quantitative assessment of the stability of the safety margin and a comparison of the performance of the systems in different positioning modes. The results of the analysis are presented in tabular form (Table 2) and graphically interpreted in the form of rH_{PL} and rV_{PL} waveforms (Figure 9).

Statistical analysis of the rH_{PL} and rV_{PL} values allowed identifying clear differences between the configurations under consideration. The solutions supported by the EGNOS

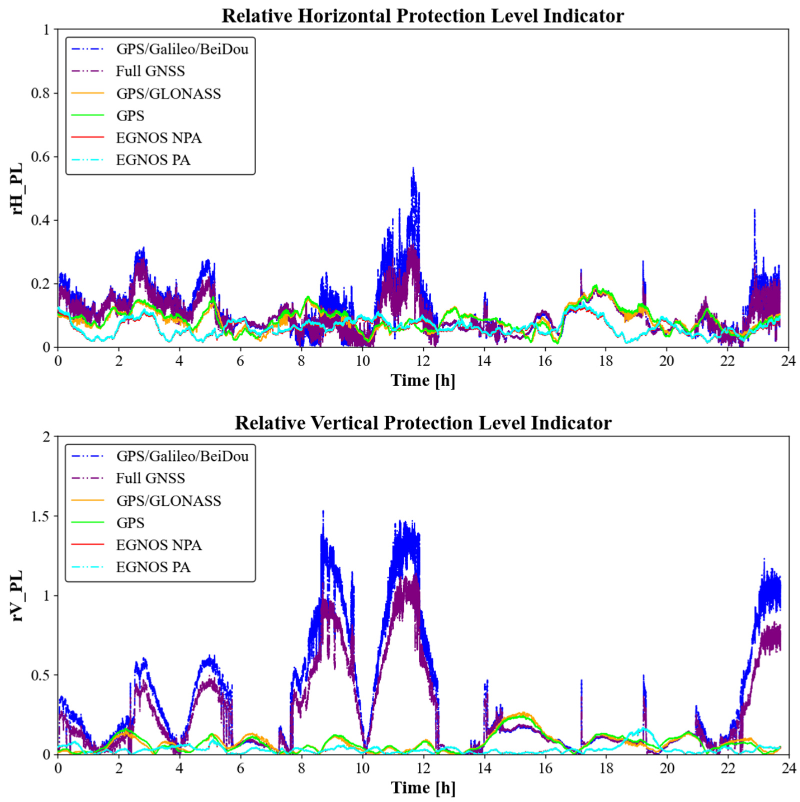

Figure 9. Daily course of relative indicators rH_{PL} (upper) and rV_{PL} (lower) for the analysed GNSS configurations

Table 2. Statistics of rHPL and rVPL indicators for the analysed GNSS configurations

Variant type	Indicator rH_{PL}		Indicator rV_{PL}	
	Maximum	Mean	Maximum	Mean
EGNOS NPA	0.137	0.06	0.166	0.030
EGNOS PA	0.143	0.062	0.167	0.030
GPS	0.196	0.086	0.243	0.067
GPS/GLONASS	0.193	0.084	0.265	0.068
GPS/Galileo/BeiDou	0.568	0.112	1.531	0.318
FULL GNSS	0.325	0.099	1.140	0.241

system (NPA and PA) gained a decisive advantage, achieving the lowest values and the highest stability for both indicators. In the horizontal plane, the average rH_{PL} values in the EGNOS modes did not exceed 0.05, while for the vertical component, the rV_{PL} values remained below 0.1 throughout the observation period. Clear differences were observed in solutions independent of the EGNOS system. Statistical analysis showed higher average values of the indicators, with rH_{PL} most often ranging from 0.1 to 0.3, while for rV_{PL}, short periods of elevated values were recorded, during which the index approached or temporarily exceeded unity, reaching values of around 1.5. This indicates periodic exceeding of the safety margin of protection for the vertical component and limited stability of integrity for these solutions.

The results obtained allow concluding that the use of the EGNOS system leads to a more stable relationship between the actual position error and the levels of protection, ensuring the greatest margin of safety necessary in landing procedures. Other configurations show limited ability to provide a stable margin of protection.

Assessment of GNSS system integrity based on Stanford charts

The analysis of proprietary relative indicators is supplemented by the use of Stanford charts. This method is commonly used in aviation due to its ability to clearly assess the compliance of position errors with acceptable limits and also allows for the visual identification of potential exceedances of the ICAO standards [38,40].

Stanford charts show the relationship between the actual position error (HPE, VPE) and the specified protection level (HPL, VPL), for which the line HPE = HPL (VPE = VPL) represents the credibility limit. The points above the straight line indicate that the system is working correctly, with the actual error not exceeding the protection level, while the points above the limit indicate a risk of loss of system integrity [38].

The following section presents Stanford plots for all analysed possibilities in relation to the horizontal plane (Figure 10) and the vertical component (Figure 11).

A comparison of the HPE/HPL Stanford graphs shows that EGNOS-assisted systems stand out in terms of positioning stability and integrity. In EGNOS NPA and EGNOS PA modes, all measurement points are clearly above the boundary line. HPE horizontal error values do not exceed 1.0–1.5 m, while the corresponding HPL protection levels remain at 7–12 m. It should be noted, however, that in the EGNOS PA mode single outliers are observed, reaching HPL values of approximately 28 m. These deviations are of a transient nature and are likely associated with short-term degradation of satellite geometry. This means that the available safety margin is used to a small extent and that there is a high level of compliance with the ICAO requirements. For the other solutions, greater point dispersion is observed. The HPE errors locally reach values of 2–5 m, with a simultaneous increase in HPL to approximately 20 m. Despite the absence of formal credibility limiting exceedances, the limited available safety margin indicates reduced credibility stability compared to the SBAS solutions.

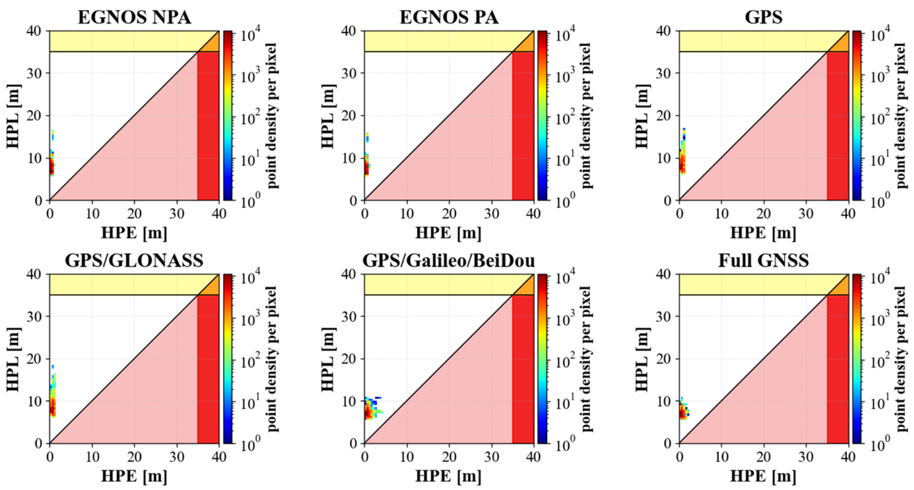

Figure 10. Stanford plots for the horizontal plane (HPE/HPL) for all analysed GNSS configurations

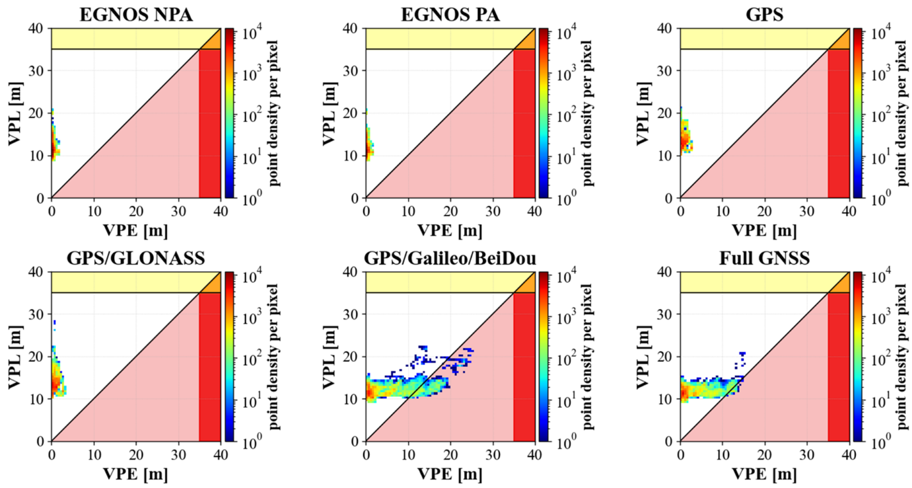

Figure 11. Stanford plots for vertical analysis (VPE/VPL) for all analyzed GNSS configurations

Analysis of Stanford plots for the VPE/VPL relationship shows significantly greater variability in vertical errors. The variants using the EGNOS system (NPA and PA) again showed a strong concentration of measurement points in the low VPE range, most often below 2 m, with simultaneous VPL protection levels of 9–15 m. This indicates a clear safety margin and high stability of the solution. In the case of autonomous solutions, the distribution of points is more dispersed. The VPE errors in the GPS variant reach about 4 m, while in multi-system modes, the VPE values locally exceed 15–20 m, with simultaneous VPL values of about 10–20 m. Although most observations remain within integrity bounds, some cases of VPE exceeding VPL occur, indicating local violations of the protection level. Consequently, the safety margin is reduced compared to EGNOS-based solutions, and the increased variability of VPE reflects higher sensitivity to signal quality disturbances. These effects are particularly evident in the GPS/Galileo/BeiDou and Full GNSS solutions and may result from inter-system differences in signal characteristics, geometry, as well as temporary degradations affecting individual constellations, which together can locally impact vertical positioning performance.

Analysis of Stanford's graphs confirms that the EGNOS-assisted solutions provide the highest and most stable level of safety in both the horizontal plane and vertical component. The results clearly indicate that, under local conditions, the EGNOS system will provide reliable and stable support that meets ICAO requirements.

Local protection level model (LPLM)

This paper proposed an original LPLM, which constitutes an original contribution to the field of GNSS integrity analysis [23,37]. The model allows protection levels to be determined for the solutions without an augmentation system, based solely on actual position errors and geometric coefficients.

The model is based on the observation of the dependence of position errors in the ENU system on satellite geometry [31, 34]. For each measurement epoch, normalised position error values were determined:

$$q_H(t) = \frac{|HPE(t)|}{PDOP(t)}, q_V(t) = \frac{|VPE(t)|}{VDOP(t)} \qquad (11)$$

The designated values enable the normalisation of position errors relative to the instantaneous geometry of satellites. The distributions of qH and qV variables (Figure 12) illustrate the variability of normalised positioning errors, reflecting their frequency of occurrence and enabling the identification of extreme values.

Based on the distributions of variables, limit values corresponding to a confidence level of p=99.9% were determined, assuming:

$$k_H = Q_{0.999}(q_H), k_V = Q_{0.999}(q_V) \qquad (12)$$

The determined values of the k_H and k_V coefficients (Table 3) serve as local safety multipliers, determining the minimum required margin of protection for the adopted receiver operating mode.

In accordance with the adopted LPLM model, the following protection levels have been determined:

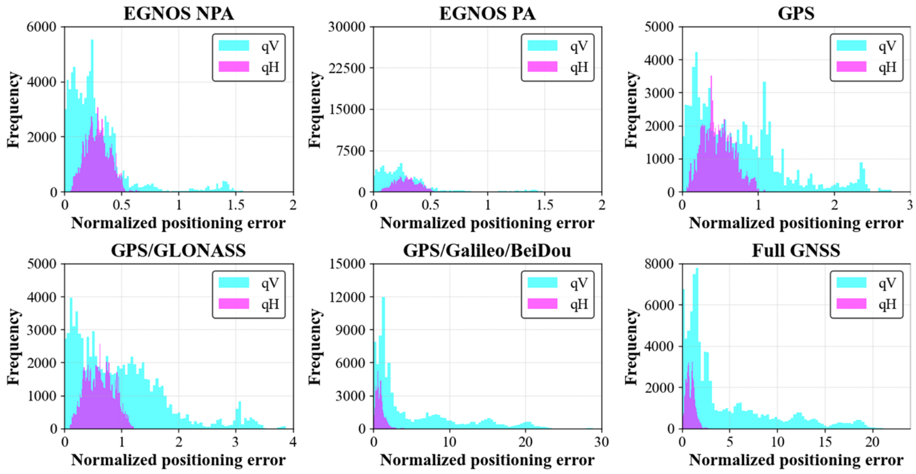

Figure 12. Distribution of normalised positioning errors q_H and q_V for all analysed GNSS configurations

Table 3. Values of local safety multipliers k_H and k_V for the adopted receiver operating mode

Variant type	Factor k_H	Factor k_V
EGNOS NPA	0.633	1.498
EGNOS PA	0.658	1.533
GPS	1.012	2.698
GPS/GLONASS	1.200	3.801
GPS/Galileo/BeiDou	4.058	28.452
FULL GNSS	2.718	20.430

$$HPL_{LPLM}(t) = k_H \cdot PDOP(t)$$
$$VPL_{LPLM}(t) = k_V \cdot PDOP(t) \quad (13)$$

The protection levels defined in this way depend solely on local signal reception conditions and the current satellite geometry. The proposed model is conservative, as the k_H and k_V coefficients are determined on the basis of extreme quantiles of the error distribution. The method used ensures that an adequate safety margin is maintained, even under the conditions of high position error variability. Additionally, the cumulative distribution function (CDF) can be applied to the LPLM-based protection levels in order to assess the statistical consistency between positioning errors and the corresponding protection bounds. This approach enables evaluation of the probability that the positioning error remains within the limits defined by the locally determined protection levels. The results confirm that the LPLM model preserves an appropriate safety margin, even under conditions of increased error variability and unfavourable satellite geometry.

The effectiveness of the model was assessed on the basis of Stanford plots. The plots show the relationship between HPE (Figure 13) or VPE

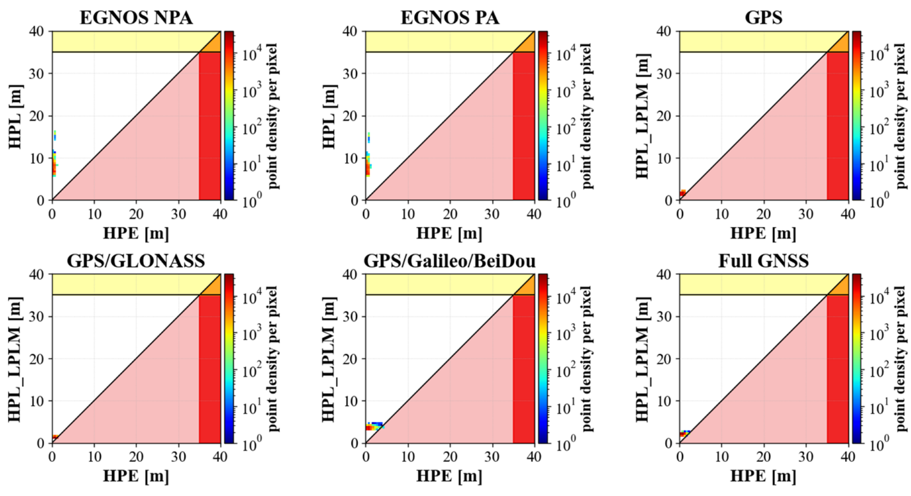

Figure 13. Stanford HPE/HPL graphs for the local protection level model (LPLM)

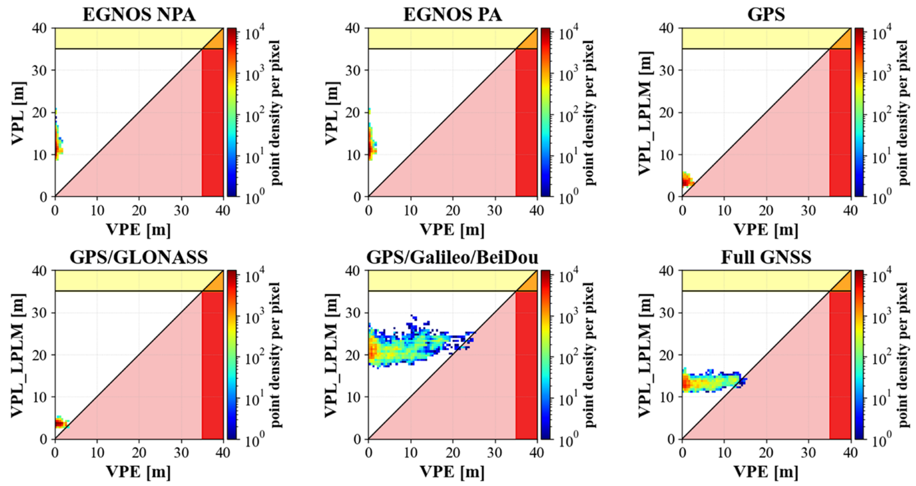

Figure 14. Stanford VPE/VPL graphs for the local protection level model (LPLM)

(Figure 14) position errors and locally determined protection levels. For the EGNOS NPA and EGNOS PA solutions, the analysis was based on the protection levels provided by the EGNOS system, without using the LPLM model.

The analysis of the results indicates that in autonomous and multi-system configurations, along with the deterioration of satellite geometry, a clear increase in the values of HPL_LPLM and VPL_LPLM is observed, indicating the correctness of the model assumptions. For the GPS/Galileo/BeiDou and Full GNSS variants, the HPL_LPLM values reached approximately 5 m, while the VPL_LPLM values increased to 15–25 m, showing the greatest variability among the variants analysed. This variability confirms the instability of the solution in the vertical direction. The variants supported by the EGNOS system were included in the comparative analysis despite the lack of the LPLM model in the graphs. However, the obtained kH and kV integrity coefficients indicate that the protection levels determined by the LPLM model did not exceed the HPL and VPL values generated operationally by the EGNOS system. In the EGNOS NPA and EGNOS PA modes, the protection levels remained at HPL of approximately 7–12 m and VPL within 9–15 m, respectively.

The proposed LPLM model is a practical solution for integrity analysis in GNSS systems operating without SBAS support. The local protection levels determined using the model are consistent with the actual dynamics of position errors and take into account the influence of satellite geometry. The conservative nature of the model results from the use of high quantiles of normalised error distributions. The model can be used to analyse the integrity of various GNSS configurations, determine protection levels in unsupported modes, and assess the compliance of autonomous solutions with ICAO standards.

CONCLUSIONS

The research confirmed that the use of the EGNOS system significantly improves the quality and integrity of GNSS positioning under the conditions typical for small airports and landing sites without ground infrastructure. The results obtained during the 24-hour measurement session indicate that EGNOS-assisted solutions are distinguished by the lowest position error variability and the highest stability of protection levels compared to other GNSS solutions. This is also confirmed by the cumulative distribution function (CDF) analysis, which shows significantly greater predictability in the SBAS modes. However, it should be emphasised that the conclusions presented refer to a single observation day. Therefore, the presented results should be treated as preliminary. It should be noted that GNSS positioning performance may vary depending on satellite geometry, ionospheric conditions, and environmental factors. Consequently, future research should include long-term observations conducted over different time periods and under varying measurement conditions in order to improve the statistical robustness and generalisation of the results. Such studies would enable a more comprehensive assessment of system stability and the repeatability of the obtained results.

The PDOP analysis shows that a more favourable satellite geometry does not directly translate into a level of integrity comparable to the EGNOS solutions. These observations were confirmed by Stanford plots, which allowed for a graphical assessment of the relationship between position errors and protection levels. The variants without an assistance system showed greater point dispersion and periodic increases in error values, leading to reduced protection levels. In contrast, the variants in the EGNOS mode maintained a high level of safety in both the horizontal plane and vertical component.

The relative rH_{PL} and rV_{PL} indicators enabled a quantitative assessment of the degree of utilisation of the available protection levels. The most favourable parameters were obtained in solutions based on the EGNOS system, for which the highest stability of the analysed indicators and limited variability over time were recorded. In contrast, the observed variability of parameters in the other variants confirms their greater susceptibility to GNSS signal interference.

The proposed LPLM is a practical method for assessing the integrity of GNSS configurations without SBAS support. The model correctly mapped local protection levels and enabled their comparison with the solutions generated in the EGNOS mode. Analysis of the results showed that autonomous systems do not provide the level of integrity required for approach procedures. The developed model shows research potential and can be used in future scientific analyses. LPLM can be used as a tool to support the assessment of positioning integrity in locations without ground infrastructure and as a basis for analysing the stability of multi-GNSS solutions under diverse observation conditions. In addition, the model can be used to compare receivers of different classes, as well as in studies involving other SBAS systems, such as WAAS or GAGAN, enabling the identification of local differences in positioning protection and integrity levels in different operating environments.

The results confirm that the EGNOS system provides real and reliable support for approach operations at uncontrolled airports and landing sites. The EGNOS system ensures compliance with performance-based navigation requirements and increases the availability and safety of GNSS-based procedures. The developed LPLM model can serve as a valuable supplement to existing methods of integrity assessment in local environments without certified SBAS support.

REFERENCES

1. Sabatini R, Moore T, Ramasamy S. Global navigation satellite systems performance analysis and augmentation strategies in aviation. Prog Aerosp Sci. 2017;95:45–98. https://doi.org/10.1016/j.paerosci.2017.10.002
2. Dautermann T. Civil air navigation using GNSS enhanced by wide area satellite based augmentation systems. Prog Aerosp Sci. 2014;67:51–62. https://doi.org/10.1016/j.paerosci.2014.01.003
3. Li X, Ge M, Dai X, Ren X, Fritsche M, Wickert J, Schuh H. Accuracy and reliability of multi-GNSS real-time precise positioning: GPS, GLONASS, BeiDou, and Galileo. J Geod. 2015;89:607–635. https://doi.org/10.1007/s00190-015-0802-8
4. Montenbruck O, Steigenberger P, Hauschild A. Multi-GNSS signal-in-space range error assessment – Methodology and results. Adv Space Res. 2018. https://doi.org/10.1016/j.asr.2018.03.041
5. Krasuski K. Application of the GPS/EGNOS solution for the precise positioning of an aircraft vehicle. Sci J Silesian Univ Technol Ser Transport. 2017;96:81–93. https://doi.org/10.20858/sjsutst.2017.96.8
6. Fellner A, Banaszek K, Trómiński P. The satellite based augmentation system - EGNOS for non-precision approach global navigation satellite system. Transport Problems. 2012;7:5–19.
7. Grunwald G, Ciećko A, Tanajewski D. Analysis of Applying the EGNOS System in APV-1 and LPV-200 Operations. IOP Conf Ser Earth Environ Sci. 2019;221. https://doi.org/10.1088/1755-1315/221/1/012075
8. ICAO. Annex 6 – Operation of Aircraft. Part I. International Civil Aviation Organization; 2018.
9. ICAO. Annex 10 – Aeronautical Telecommunications. Volume II. International Civil Aviation Organization; 2016.
10. ICAO. Doc 8168. Procedures for Air Navigation Services – Aircraft Operations. Vol II. 2020.
11. Wang Y, Jin B, Chen S. The Service Performance Evaluation of Different Satellite Based Augmentation Systems. 2015. https://doi.org/10.1007/978-3-662-46635-3_26
12. Ciećko A, Grunwald G. Examination of autonomous GPS and GPS/EGNOS integrity and accuracy for aeronautical applications. Period Polytech Civ Eng. 2017;61:920–928. https://doi.org/10.3311/ppci.10022
13. Krasuski K, Wierzbicki D. Monitoring aircraft position using EGNOS data for the SBAS APV approach to the landing procedure. Sensors. 2020;20. https://doi.org/10.3390/s20071945
14. Beldjilali B, Kahlouche S, Tabti L. Assessment of EGNOS performance for civil aviation flight phase in

the edge coverage area. Int J Aviat Aeronaut Aerosp. 2020;7. https://doi.org/10.15394/ijaaa.2020.1479

15. Specht M. Consistency of the empirical distributions of navigation positioning system errors with theoretical distributions. Sensors. 2020;21. https://doi.org/10.3390/s21010031
16. Grunwald G, Ciećko A, Krasuski K, Kaźmierczak R. The GPS/EGNOS Positioning Quality in APV-1 and LPV-200 flight procedures. Commun Sci Lett Univ Zilina. 2021;23:E23–34. https://doi.org/10.26552/com.C.2021.2.E23-E34
17. Krasuski K, Mrozik M, Wierzbicki D, Ćwiklak J, Kozuba J, Ciećko A. Designation of the quality of EGNOS+SDCM satellite positioning in the approach to landing procedure. Appl Sci. 2022;12. https://doi.org/10.3390/app12031335
18. Mrozik M, Kozuba J, Krasuski K, Ćwiklak J, Bakuła M, Ciećko A, et al. Analysis of the accuracy of EGNOS+SDCM positioning in aerial navigation. Arch Transport. 2022. https://doi.org/10.5604/01.3001.0016.2028
19. Tossaint M, Samson J, Toran F, Ventura-Traveset J, Hernández-Pajares M, Juan J, et al. The Stanford – ESA integrity diagram. Navigation. 2007;54:153–162. https://doi.org/10.1002/j.2161-4296.2007.tb00401.x
20. Racelis D, Joerger M. Evaluating new and current horizontal protection levels in the baseline ARAIM algorithm. ION GNSS+. 2022. https://doi.org/10.33012/2022.18360
21. Specht M. Statistical distribution analysis of navigation positioning system errors. Sensors. 2020;20. https://doi.org/10.3390/s20247144
22. Specht M. Determination of navigation system positioning accuracy using the reliability method. Remote Sens. 2021;13:4424. https://doi.org/10.3390/rs13214424
23. Liu B, Gao Y, Gao Y, Wang S. HPL calculation improvement for Chi-squared residual-based ARAIM. GPS Solut. 2022;26. https://doi.org/10.1007/s10291-021-01220-0
24. Wang K, El-Mowafy A, Qin W, Yang X. Integrity monitoring of PPP-RTK positioning; Part I. Remote Sens. 2021;14:44. https://doi.org/10.3390/rs14010044
25. Septentrio NV. PolaRx5e Reference Receiver User Manual. Leuven; 2021.
26. ICAO. Doc 9613. Performance-based Navigation (PBN) Manual. 2008.
27. Septentrio NV. PP-SDK Software User Guide. Leuven; 2022.
28. Niu X, Chen Q, Zhang Q, Zhang H, Niu J, Chen K, et al. Using Allan variance to analyze the error characteristics of GNSS positioning. GPS Solut. 2014;18:231–242. https://doi.org/10.1007/s10291-013-0324-x
29. Rovira-Garcia A, Ibáñez-Segura D, Pérez R, Juan J, Sanz J, González-Casado G. Assessing the quality of ionospheric models through GNSS positioning error. GPS Solut. 2019;24. https://doi.org/10.1007/s10291-019-0918-z
30. Bakota M, Kos S, Mrak Z, Brčić D. Improving GNSS geodetic position by reducing residual tropospheric error. Remote Sens. 2022;15:162. https://doi.org/10.3390/rs15010162
31. Huang B, Yao Z, Cui X, Lu M. Dilution of precision analysis for GNSS collaborative positioning. IEEE Trans Veh Technol. 2016;65:3401–3415. https://doi.org/10.1109/tvt.2015.2436700
32. Kabir M, Lee S, Shin W. Performance evaluation of GNSS positioning with geometric dilution of precision. ICTC. 2022. https://doi.org/10.1109/ictc55196.2022.9953014
33. Verma P, Hajra K, Banerjee P, Bose A. Evaluating PDOP in multi-GNSS environment. IETE J Res. 2019. https://doi.org/10.1080/03772063.2019.1666750
34. Zheng S, Zhou L, Lu C, Wang W, Lv G. Global GNSS PDOP calculation method based on hexagonal discrete grid. Int J Geogr Inf Sci. 2025. https://doi.org/10.1080/13658816.2024.2446537
35. Lai Y, Blanch J, Walter T. Troposphere delay model error analysis with application to vertical protection level calculation. ION ITM. 2023. https://doi.org/10.33012/2023.18615
36. Tang T, Xiang Y, Lyu S, Zhao Y, Yu W. Statistical modeling of PPP-RTK derived ionospheric residuals. Electronics. 2025. https://doi.org/10.3390/electronics14122340
37. Pereira V, Monico J, Camargo P. Estimation and analysis of protection levels for precise approach. Bol Ciênc Geod. 2021. https://doi.org/10.1590/s1982-21702021000s00010
38. Du Y, Wang J, Rizos C, El-Mowafy A. Vulnerabilities and integrity of precise point positioning. Satellite Navigation. 2021. https://doi.org/10.1186/s43020-020-00034-8
39. Kim E, Song J, Shin Y, Kim S, Son P, Park S, et al. Fault-free protection level equation for CLAS PPP-RTK. Sensors. 2022;22. https://doi.org/10.3390/s22093570
40. Mrozik M, Kozuba J, Krasuski K, Ćwiklak J, Bakuła M, Beldjilali B. New strategy for designation of the integrity parameter in SBAS positioning in air transport. Sci J Silesian Univ Technol Ser Transport. 2024. https://doi.org/10.20858/sjsutst.2024.122.13